doi:10.2533/chimia.2008.287 CHIMIA **2008**, *62*, No. 4

Chimia 62 (2008) 287–290

ISSN 0009–4293

EXAFS Structural Determination of the $Pt_2(P_2O_5H_2)_4^{4-}$ Anion in Solution

Renske M. van der Veen[§*ab], Christopher J. Milne[a], Van-Thai Pham[a], Amal El Nahhas[a], Julia A. Weinstein[c], Jonathan Best[c], Camelia N. Borca[b], Christian Bressler[a], and Majed Chergui*[a]

[§]SCS Poster Prize Winner

Abstract: We present the first structural determination of the $Pt_2(P_2O_5H_2)_4^{4-}$ anion in solution by analyzing the extended X-ray absorption fine structure (EXAFS) spectrum of the Pt L_{III} edge. The data could be fit with a simple model involving single and multiple scattering paths to near and far P-atoms, bridging O-atoms, and the other Pt-atom in the binuclear complex. A Pt–Pt distance of 2.876(28) Å and a Pt–P bond length of 2.32(4) Å are obtained. These values are in line with distances found in previous X-ray diffraction studies. The assignment of the EXAFS spectrum of the $Pt_2(P_2O_5H_2)_4^{4-}$ anion in its ground state is required for future time-resolved X-ray absorption measurements with the goal of determining the structure and dynamics of the complex in the $^{1,3}A_{2u}$ excited states.

Keywords: Diplatinum complexes · EXAFS · Molecular structures

1. Introduction

Observation of the making and breaking of bonds in the course of a chemical reaction is the dream of every chemist. The advent of femtosecond (fs) lasers in the 1980s brought about a fully new field of research: femtochemistry, *i.e.* atomic-scale dynamics of the chemical bond which fundamentally occurs on the time scale of tens to hundreds of fs.[1] The pump-probe scheme, in which a short laser (pump) pulse excites the sample, while another short (probe) pulse detects the pump-induced changes in the sample at a later time, has allowed the observation of nuclear motion in 'real-time' over the course of a chemical reaction, a molecular vibration or rotation, in both isolated systems and in the condensed phase.[1] The pump and probe pulses are commonly in the UV/visible wavelength range, exciting valence electronic molecular transitions. However, retrieving structural information from optical spectroscopy is possible only in a few rare cases (*e.g.* diatomic molecules and a few triatomic ones) for which potential energy surfaces are in general known. For more complex systems, detection of transient molecular structures is only possible based on methods that probe atomic coordinates directly, such as X-ray absorption spectroscopy and X-ray diffraction.[2]

Time-resolved X-ray absorption spectroscopy (XAS) is a recently developed technique to study transient structures of photo-excited coordination complexes.[3] Core transitions from the inner shell of an atom in a molecule give rise to so-called edge features, which are located near the ionization threshold of the core transition. In an isolated atom, the spectrum above the edge is monotonous, but if the atom is embedded in a molecule, a crystal or a protein, modulations show up due to the scattering of the photoelectron with the neighbouring atoms, and the interference of the back-scattered with the outgoing photoelectron waves.[4] These modulations contain local structural information, and are divided in two regions: the X-ray near-edge absorption fine structure (XANES) in the low energy region around and just above (up to approx. 50 eV) the edge jump, and the extended X-ray absorption fine structure (EXAFS) well above the edge spectra. XANES features are due to multiple scattering events, while EXAFS ones are due to single scattering events, and are therefore simpler to interpret. Here we concentrate on the latter.

Just as in optical pump-probe spectroscopy, our experimental strategy is based on the recording of transient X-ray absorption spectra, which is the difference between the X-ray absorption spectrum of the laser-excited sample minus that of the unexcited sample.[3] Therefore an obvious and indispensable input in these studies is the measurement of the EXAFS spectrum of the molecule in its ground state, and there from, the determination of its structure. Using picosecond XAS, our group determined the structural changes upon light-induced intramolecular electron transfer in $[Ru^{II}(bpy)_3^{2+}]$[3b] and the $\Delta S = 2$ spin change in $[Fe^{II}(bpy)_3^{2+}]$.[3c–d] For the first time, we have recently extended these studies to the femtosecond time domain.[3e]

It is on the background of these activities that we turned to the case of the binuclear Pt(II) complex $Pt_2(P_2O_5H_2)_4^{4-}$ (abbreviated $Pt_2(pop)_4^{4-}$, Fig. 1). This system is interesting because of its strongly luminescent excited $^3A_{2u}$ state which has a life time of ~10 μs in solution at room temperature.[5]

*Correspondence: R. M. van der Veen[a], Prof. Dr. M. Chergui[a]
Tel.: +41 56 310 5362, +41 21 693 0457
Fax: +41 56 310 4413, +41 21 693 0422
E-mail: renske.vanderveen@psi.ch, majed.chergui@epfl.ch
[a]École Polytechnique Fédérale de Lausanne
Laboratoire Spectroscopie Ultrarapide
BSP/Cubotron 427
CH-1015 Lausanne
[b]Paul Scherrer Institut
Swiss Light Source
CH-5232 Villigen PSI
[c]The University of Sheffield
Department of Chemistry
S3 7HF Sheffield, UK

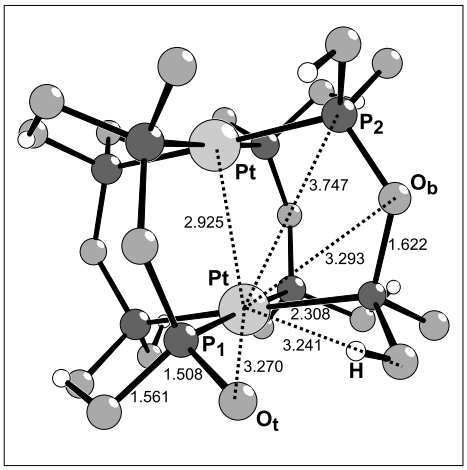

Fig. 1. Molecular structure of $Pt_2(P_2O_5H_2)_4^{4-}$. Distances (in Å) belong to the structural model that is used for the fit of the EXAFS data in Section 4 (taken from crystal data in ref. [6]). P_1 = near P atom; P_2 = far P atom; O_b = bridging O atom; O_t = terminal O atom. All P-atoms are equivalent; all O_b atoms are equivalent; the O_t atoms fall into two equivalent sets.

The formal bond order changes from 0 to 1 in the $^1A_{1g} \rightarrow {}^1A_{2u}$ ($d\sigma^* \rightarrow p\sigma$) transition, causing the Pt–Pt bond to contract considerably and the structure is considered to be the same in the $^3A_{2u}$ as in the $^1A_{2u}$ excited state.[5g–h] A decrease in Pt–Pt distance of ~0.2–0.3 Å in the long-lived $^3A_{2u}$ excited state has been deduced from resonance Raman spectroscopy and Franck-Condon analysis of the vibrational fine structure of the absorption and emission spectra at low temperature.[5c–f] We are interested in probing the structural changes in the excited state as they occur, as well as the accompanying intersystem crossing by means of time-resolved XAS.

Only few X-ray studies of either the ground state or the triplet state structures have been carried out. X-ray diffraction studies of the $K_4Pt_2(pop)_4$ crystal were first carried out by Sadler and co-workers, who found the Pt–Pt distance to be 2.925 Å.[6] This value is close to more recent X-ray diffraction determinations by Coppens and co-workers, (2.913 Å tetraethylammonium salt),[7a,b] and Ohashi and co-workers (2.942–2.973 Å with different organic counter ions).[7c] However, Sadler also recorded NMR spectra of the $Pt_2(pop)_4^{4-}$ anion in solution showing that its symmetry is reduced in the crystal due to Coulomb interactions of the O-atoms with the K^+-ions,[6] and it is not clear if, and to what extent, this distortion affects the Pt–Pt bond distance. A time-resolved EXAFS study in solution reported a shortening of the Pt–phosphorus and Pt–oxygen distances in the $^3A_{2u}$ state, but was not sensitive to the Pt–Pt bond. The authors used therefore the spectroscopically determined Pt–Pt distance of 2.75 Å[8] to derive a contraction of 0.52 Å of the planes through four P-atoms along the Pt–Pt axis, implying a ground state Pt–Pt distance of 3.27 Å,[9] substantially larger than that measured in the crystal. In deriving this contraction, the authors made the assumption that the Pt atoms stay attached to the plane of the P atoms, which must not be generally true. Our aim here is to reexamine the structure of $Pt_2(pop)_4^{4-}$ in solution using EXAFS spectroscopy, as a preliminary step to a picosecond and later, femtosecond investigation of the excited state structural dynamics.

2. Experimental

$(TBA)_4[Pt_2(P_2O_5H_2)_4]$ samples were prepared by published procedures.[10] All experiments were performed at room temperature and no sample degradation was observed after the experiments as checked by UV/Vis absorption spectroscopy.

The EXAFS measurements were performed using a standard setup at the hard X-ray X05LA beam line of the Swiss Light Source. Two ion chambers filled with 1 bar of He were used for detection of the incoming and transmitted X-ray flux. A solution of $(TBA)_4[Pt_2(P_2O_5H_2)_4]$ in ethanol (18 mM) was contained in a quartz capillary with a path length of 2 mm and a wall thickness of 10 µm. The integration time per data point was set to 1 s and in total two EXAFS scans were recorded and averaged. EXAFS data analysis was done using version 1.2.10 of the program package IFEFFIT which includes version 6.02L of FEFF.[11a–b]

3. EXAFS Analysis

The X-ray absorption $\mu(E)$ as a function of energy is given by

$$\mu(E) = \ln\left(\frac{I_0}{I_T}\right) \qquad (1)$$

where I_0 is the incoming X-ray flux and I_T is the transmitted X-ray flux after the sample. For the EXAFS analysis it is necessary to generate the normalized fine structure $\chi(k) = \mu(k) - \mu_0(k)/\mu_0$, where $\mu_0(k)$ is the background function and μ_0 is the edge step $\mu_0(k=0)$. The magnitude of the wave vector k is given by

$$k = \sqrt{\frac{2m_e}{\hbar^2}\left(E - E_0\right)} \qquad (2)$$

where E_0 is the energy threshold for an electron ejected from the absorbing atom. The experimental $\chi(k)$ corresponds directly to the theoretical EXAFS equation expressed as a scattering path expansion[4,11b]

$$\chi(k) = \sum_\Gamma \frac{N_\Gamma {S_0}^2 F_\Gamma(k)}{k {R_\Gamma}^2} e^{-2\sigma_\Gamma{}^2 k^2} e^{-2R_\Gamma/\lambda(k)} \sin\left(2kR_\Gamma + \varphi_\Gamma(k)\right) \qquad (3)$$

with the scattering path index Γ, the number of equivalent scattering paths N_Γ, the amplitude reduction factor ${S_0}^2$, the scattering factor $F_\Gamma(k)$, the half-path distance R_Γ, the squared Debye-Waller (DW) factor $\sigma_\Gamma{}^2$, the mean free path $\lambda(k)$ and the total phase shift $\varphi_\Gamma(k)$. The oscillatory structure of an EXAFS spectrum is caused by the last term in Eqn. (3) and can phenomenologically be seen as the interference of the outgoing and backscattered photoelectron waves. Fourier transformation (FT) of Eqn. (3) yields direct information about the distances between atoms *via* the half-path distances R_Γ, assuming that the other parameters for each path are known. Therefore, the FT of $\chi(k)$ is commonly called the pseudo radial distribution function (RDF). From a given input structure, the EXAFS analysis program FEFF computes all possible scattering pathways from the central atom to its neighbouring atoms that are smaller than a given distance, as well as their scattering factors $F_\Gamma(k)$, their phase shifts $\varphi_\Gamma(k)$, and the electron mean free path $\lambda(k)$.[11] The other parameters, ${S_0}^2$, $\sigma_\Gamma{}^2$, ΔR_Γ (the change in half-path length relative to the model compound) and E_0 (determining k *via* Eqn. (2)), are evaluated in the fitting procedure according to a specific fitting model.

4. Results and Discussion

Fig. 2a shows the normalized X-ray absorption $\mu(E)$ as a function of photon energy around the Pt L_{III} edge (11.564 keV). Normalization was performed by subtracting pre- and post-edge lines from the spectrum and dividing by the value of the post-edge line at the edge energy position.[11] The dotted curve in Fig. 2a represents the background function $\mu_0(E)$ that is used to generate the normalized fine structure $\chi(k)$, which is shown in Fig. 2b in the range 2.9–13 $Å^{-1}$ (weighted by k^2).

The choice of a suitable model system as a starting point for the FEFF calculation should be carefully made. As mentioned in the introduction, the symmetry of the $[Pt_2(pop)_4]^{4-}$ anion is reduced in the crystal due to Coulomb interactions between O atoms and positive counter ions which are absent in solution. Therefore, we cannot use the crystal structure as a model system to fit the EXAFS data in Fig. 2. Instead, we use a structure with D_{4h} symmetry of the $Pt_2P_8O_4$

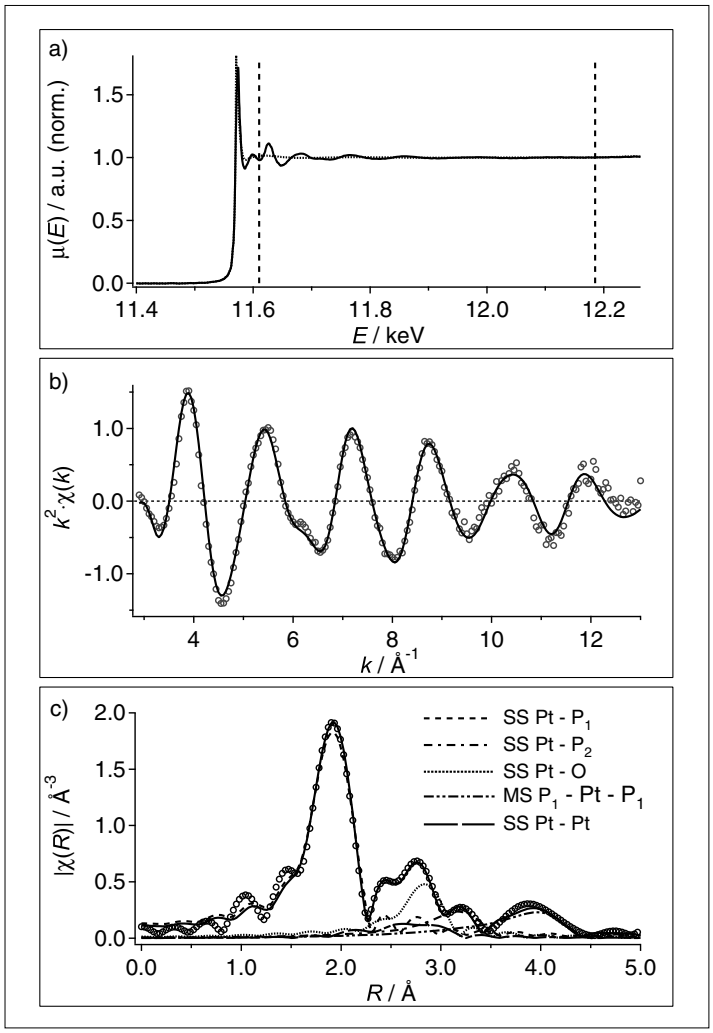

Fig. 2. a) Normalized X-ray absorption spectrum $\mu(E)$ of $(TBA)_4[Pt_2(P_2O_5H_2)_4]$ in ethanol. The dotted curve is the background function and the two dashed vertical lines denote the FT range. b) $\chi(k)$ weighted with k^2 (open circles) and the fit after back-FT (solid line). c) Magnitude of the FT of $k^2 \cdot \chi(k)$ (open circles), the fit (solid line), and the contributions from different scattering paths (dashed lines; SS = single scattering path; MS = multiple scattering path; P_1 = near P atoms; P_2 = far P atoms; O = bridging O atoms). No phase correction is applied to the *R*-axis.

Table. Comparison between bond lengths in Å determined in this work and in previous studies

	This work[a]	XRD[b]	XRD[c]	XRD[d]	DFT[e]
Pt–Pt	2.876(28)	2.925(1)	2.9126(2)	2.9419(3)	3.039
Pt–P_1	2.32(4)	2.334(4)	2.3274(6)	2.3338(10)	2.393
Pt–P_1'[f]		2.307(4)			

[a] $Pt_2(pop)_4^{4-}$ in ethanol; [b] X-ray diffraction (XRD), $K_4[Pt_2(pop)_4]\cdot 2H_2O$;[6] [c] $(TEA)_2H_2[Pt_2(pop)_4]$;[7a] [d] $(TBA)_4[Pt_2(pop)_4]$;[7c] [e] Density functional theory (DFT) calculation;[7b] [f] the molecule in the solid state exhibits two sets of equivalent P_1 atoms because of Coulomb interactions in the crystal. The Pt–P_1 distances in the organic TEA and TBA crystals are less affected by this. All P atoms become equivalent in solution.

'cube', with the Pt atoms slightly out of the P_4 plane, with four equivalent bridging O atoms, and with two sets of terminal O atoms with P–O bond lengths for single and double P–O bonds, respectively (see Fig. 1). The atomic coordinates were taken from the crystal structure data of $K_4[Pt_2(pop)4]$, except that the symmetry was increased as described above.[6] The fitting model uses in total ten fitting parameters: S_0^2, E_0, ΔR_{Pt-P1}, σ_{Pt-P1}^2, ΔR_{Pt-P2}, σ_{Pt-P2}^2, ΔR_{Pt-O}, σ_{Pt-O}^2, ΔR_{Pt-Pt} and σ_{Pt-Pt}^2, where Pt–P_1 denotes the single scattering (SS) path to the nearest P atoms, Pt–P_2 denotes the SS path to the far P atoms and Pt–O denotes the SS path to the bridging O atoms. The parameters for the four-legged collinear multiple-scattering path involving the absorbing Pt atom and two opposite P1 atoms, with one forward scattering event at the Pt atom, is expressed in terms of single-scattering parameters ($\Delta R_{MS} = 2\cdot \Delta R_{Pt-P1}$, $\sigma_{MS}^2 = 2\cdot \sigma_{Pt-P1}^2$). In addition, in order to reduce the number of free fitting parameters, the squared DW factor for the Pt–Pt SS path is calculated independently by making use of the Pt–Pt vibration frequency $\bar{\nu} = 118$ cm^{-1} in solution.[5d] The squared DW factor can be expressed as[12]

$$\sigma^2 = \frac{h}{8\pi^2 \mu \nu} \coth\left(\frac{h\nu}{2kT}\right) \qquad (4)$$

where μ is the reduced mass, T is the temperature, and ν is the vibrational frequency (in s^{-1}). The force constant $K = 4\pi^2\mu\nu^2 = 0.77$ mdyn/Å for the Pt–Pt vibration including the restoring force from the bridging ligands is taken from ref. [8] in order to derive the reduced mass μ. In this way $\sigma_{Pt-Pt}^2 = 0.0055$ Å^2 is calculated, which is fixed to this value in the fit of the EXAFS data.

The data is fit in *R*-space after FT using a Hanning window over the *k*-range 3.3–12.7 Å^{-1}. The region fit in *R*-space spans from 1.1 to 4.9 Å (distances without phase correction). The FTs of the *k*, k^2 and k^3 weighted $\chi(k)$ data are fit simultaneously in order to reduce the correlation between parameters with different *k*-dependences. The fit to the data is shown in Fig. 2c. The contributions of the various scattering paths are shown in the plot also. The main peak around 1.9 Å is due to SS to near P atoms. Three other distinct peaks around 2.7, 3.2 and 3.9 Å are composed of scattering contributions from the bridging O atoms, the far P atoms and MS *via* the near P atoms, respectively. As previously noted by Thiel *et al.*,[9] the contribution from Pt–Pt SS is small despite the heavy Pt atoms. This is mainly due to the fact that the Pt–Pt path has degeneracy 1 (compared to the degeneracy 4 of scattering to the bridging O atoms) and to the relatively large DW factor (*vide ante*). Nevertheless, we can infer a Pt–Pt distance of 2.876(28) Å, which is slightly smaller than the values reported for crystals.[6,7,13] In addition, it might seem unrealistic to exclude the terminal O atoms from the fitting model as is done here. However, inclusion of the SS path to these O atoms does not significantly improve the fit statistics, while largely increasing the uncertainties of all other fitting parameters. This is explained by the fact that the terminal O atoms are probably very flexible in solution, as they can be involved in hydrogen bonding with other P–O groups and with

surrounding solvent molecules. Hydrogen bonding within the molecule delocalizes the charge over P and terminal O atoms so that the P–O bond length is ill-defined. Consequently, the DW factors (which include both thermal vibration and 'static' disorder) are sufficiently large to make the contribution of these scattering paths negligible. Important to note is that the collinear MS path involving the near P atoms and a forward scattering event is effectively the only path that contributes to the peak around 3.9 Å. After back-FT of the fit in the range 1.1–4.9 Å, $\chi(k)$ is obtained, which is shown together with the original data in Fig. 2b. The fit agrees very well with the experimental data. It should be noted that the wiggles below 1.5 Å in Fig. 2c are caused by slow oscillations of the background function. They do not significantly contribute to the FT above 1.5 Å.

The values of the fitting parameters obtained from the fit are as follows: S_0^2 = 0.98(4), E_0 = 8.4(5) eV, ΔR_{Pt-P1} = 0.013(4) Å, σ_{Pt-P1}^2 = 0.0034(4) Å^2, ΔR_{Pt-P2} = −0.083(16) Å, σ_{Pt-P2}^2 = 0.011(2) Å^2, ΔR_{Pt-O} = −0.027(12) Å, σ_{Pt-O}^2 = 0.0012(11) Å^2, ΔR_{Pt-Pt} = −0.050(28) Å (changes in distance ΔR are relative to the distances presented in Fig. 1). The uncertainties of and the correlations between different parameters, as determined by the fitting program, are fairly large. This is a common problem in cases where many scattering paths have similar distances and thus contribute to the same region in *R*-space (Pt–O_b, Pt–O_t and Pt–Pt have very similar distances, see Fig. 1). Unfortunately, this is unavoidable without including more external information such as temperature dependence of the DW factors. In the Table, the absolute Pt–Pt and Pt–P_1 bond lengths inferred from the above ΔR fit parameters are compared with the distances from X-ray diffraction measurements. The bond lengths are in good agreement, although the Pt–Pt distance in solution, 2.876 Å, seems to be slightly smaller than that in the crystals, 2.913–2.942 Å. One possible explanation for the shorter Pt–Pt distance in solution would be the formation of hydrogen bonds between the filled highest molecular dσ* orbital and the slightly positively charged H atoms of the ethanol solvent. Partial electron transfer from the anti-bonding dσ* orbital to the solvent causes a reduction of the Pt–Pt bond length. However, more measurements in different solvents would be necessary to strengthen this speculative explanation. The question is whether the difference in Pt–Pt bond lengths is significant. Our Pt–Pt distance is only indicative, due to overlapping contributions of different scattering paths, high correlations between the parameters and an independently derived DW factor for the Pt–Pt scattering path.

5. Conclusions and Outlook

High-quality EXAFS spectra of $Pt_2(pop)_4^{4-}$ were recorded and could be fit with a fairly simple model including single- and multiple-scattering paths to near and far P atoms, bridging O atoms and the Pt atom. The fit shows very good correspondence to the experimental data. However, Pt–O and Pt–Pt distances are very similar, which causes their scattering contributions to overlap. As a consequence the fitting parameters involving scattering to O and Pt atoms could not be determined with great accuracy. Nevertheless, the main peaks in the Fourier transform of the EXAFS data can be uniquely assigned to distinct distances in the molecule. This is important in view of the time-resolved X-ray measurements where large structural changes are expected after excitation of the $^1A1g \rightarrow {}^1A_{2u}$ (dσ* → pσ) transition.

The oxidized complex $Pt_2(P_2O_5H_2)_4X_2^{2-}$ (X = I, Cl, Br) can be seen as a structural model system for the $^1A_{2u}$ excited state.[14] Removing two electrons from the anti-bonding dσ* orbital gives a formal Pt–Pt bond order of 1 as is expected in the $^1A_{2u}$ excited state of $Pt_2(P_2O_5H_2)_4^{4-}$. Future EXAFS measurements on $Pt_2(P_2O_5H_2)_4X_2^{2-}$ will show what changes in the spectrum can be expected upon increasing the Pt–Pt bonding order by 1.

Acknowledgements

We thank D. Grolimund, R. Abela, M. Janousch and B. Ravel for helpful discussions and we thank A. Vlček and J. K. Nagle for providing us with the samples. This work is supported by the Swiss National Science Foundation (SNF) *via* contracts 110469, 105239, 116533 and by the Staatssekretariat für Bildung und Forschung (SBF) *via* contract C06.0016, in the framework of the COST D35 Action.

Received: February 25, 2008

[1] A. H. Zewail, 'Femtochemistry: Ultrafast Dynamics of the Chemical Bond', World Scientific Publishing Company, **1994**, Vol. I and II.

[2] a) J. M. Cole, *Chem. Soc. Rev.* **2004**, *33*, 501; b) R. Neutze, R. Wouts, S. Techert, J. Davidsson, M. Kocsis, A. Kirrander, F. Schotte, M. Wulff, *Phys. Rev. Lett*. **2001**, *87*, 195508.

[3] a) C. Bressler, M. Chergui, *Chem. Rev*. **2004**, *104*, 1781; b) W. Gawelda, M. Johnson, F.M.F. de Groot, R. Abela, C. Bressler, M. Chergui, *J. Am. Chem. Soc*. **2006**, *128*, 5001; c) W. Gawelda, V.-T. Pham, M. Benfatto, Y. Zaushitsyn, M. Kaiser, D. Grolimund, S. L. Johnson, R. Abela, A. Hauser, C. Bressler, M. Chergui, *Phys. Rev. Lett.* **2007**, *98*, 057401; d) W. Gawelda, A. Cannizzo, V.-T. Pham, A. El Nahhas, C. J. Milne, R. van der Veen, C. Bressler, M. Chergui, *Chimia* **2007**, *61*, 179; e) C. Bressler, C. J. Milne, V.-T. Pham, A. El Nahhas, R. M. van der Veen, W. Gawelda, S. L. Johnson, P. Beaud, D. Grolimund, C. N. Borca, G. Ingold, R. Abela, M. Chergui, to be published.

[4] 'X-ray Absorption – Principles, Applications, Techniques of EXAFS, SEXAFS and XANES', Eds. D.C. Koningsberger, R. Prins, Wiley, New York, **1988**.

[5] a) R. P. Sperline, M. K. Dickson, D. M. Roundhill, *J. Chem. Soc. Chem. Commun.* **1977**, 62; b) C.-M. Che, L. G. Butler, H. B. Gray, *J. Am. Chem. Soc*. **1981**, *103*, 7796; c) W. A. Fordyce, J. G. Brummer, G. A. Crosby, *J. Am. Chem. Soc*. **1981**, *103*, 7061; d) C.-M. Che, L. G. Butler, H. B. Gray, R. M. Crooks, W. H. Woodruff, *J. Am. Chem. Soc.* **1983**, *105*, 5492; e) S. F. Rice, H. B. Gray, *J. Am. Chem. Soc*. **1983**, *105*, 4571; f) K. H. Leung, D. L. Phillips, C.-M. Che, V. M. Miskowski, *J. Ram. Spectr.* **1999**, *30*, 987; g) A. E. Stiegman, S. F. Rice, H. B. Gray, V. M. Miskowski, *Inorg. Chem.* **1987**, *26*, 1112; h) S. J. Milder, B. S. Brunschwig, *J. Phys. Chem.* **1992**, *96*, 2189.

[6] M. A. Filomena Dos Remedios Pinto, P. J. Sadler, S. Neidle, M. R. Sanderson, A. Subbiah, R. Kuroda, J. *Chem. Soc., Chem. Comm.* **1980**, 13.

[7] a) C. D. Kim, S. Pillet, G. Wu, W. K. Fullagar, P. Coppens, *Acta Cryst.* **2002**, *A58*, 133; b) I. V. Novozhilova, A. V. Volkov, P. Coppens, *J. Am. Chem. Soc.* **2003**, *125*, 1079; c) N. Yasuda, H. Uekusa, Y. Ohashi, *Bull. Chem. Soc. Jpn*. **2004**, *77*, 933.

[8] P. Stein, M. K. Dickson, D. M. Roundhill, *J. Am. Chem. Soc.* **1983**, *105*, 3489.

[9] D. J. Thiel, P. Livins, E. A. Stern, A. Lewis, *Nature* **1993**, *362*, 40.

[10] C.-M. Che, L. G. Butler, P. J. Grunthaner, H. B. Gray, *Inorg. Chem*. **1985**, *24*, 4662.

[11] a) B. Ravel, M. Newville, *J. Synchr. Rad.* **2005**, *12*, 537; b) M. Newville, 'IFEFFIT' **2007**, *http://cars.uchicago.edu/ifeffit*; c) B. Ravel, 'EXAFS data analysis with FEFF and IFEFFIT' **2000**, *http://feff.phys.washington.edu*

[12] S. J. Cyrin. 'Molecular Vibrations and Mean Square Amplitudes' Elsevier, Amsterdam, **1968**, p 77.

[13] R. E. Marsh, F. H. Herbstein, *Acta Cryst*. **1983**, *B39*, 280.

[14] C.-M. Che, F. H. Herbstein, W. P. Schaefer, R. E. Marsh, H. B. Gray, *J. Am. Chem. Soc*. **1983**, *105*, 4604.